"Sloppy" nuclear energy density functionals. II. Finite nuclei

Nikšić, Tamara; Imbrišak, Marko; Vretenar, Dario

Download date / Datum preuzimanja: **2022-06-07**

"Sloppy" nuclear energy density functionals. II. Finite nuclei

T. Nikšić, M. Imbrišak, and D. Vretenar

Department of Physics, Faculty of Science, University of Zagreb, HR-10000 Zagreb, Croatia

A study of parameter sensitivity of nuclear energy density functionals, initiated in the first part of this work [Nikšić and Vretenar, [Phys. Rev. C **94**, 024333 (2016)](#)], is extended by the inclusion of data on ground-state properties of finite nuclei in the application of the manifold boundary approximation method (MBAM). Density functionals used in self-consistent mean-field calculations, and nuclear structure models based on them, are generally "sloppy" and exhibit an exponential range of sensitivity to parameter variations. Concepts of information geometry are used to identify the presence of effective functionals of lower dimension in parameter space associated with parameter combinations that can be tightly constrained by data. The MBAM is used in an iterative procedure that systematically reduces the complexity and dimension of parameter space of a sloppy functional, with properties of nuclear matter and data on finite nuclei determining not only the values of model parameters but also the optimal functional form of the density dependence.

I. INTRODUCTION

The complexity of internucleon interactions in the nuclear medium, the interplay between single-nucleon and collective degrees of freedom, and finite-size effects make a unified treatment of the nuclear many-body problem in a single theoretical framework very difficult. Nuclear energy density functionals (EDFs), and various collective models based on them, have emerged as the most promising unified approach for a global description of nuclear structure phenomena over the entire nuclear chart. Whether nuclear EDFs are by construction microscopic, semiempirical, or fully phenomenological, their various implementations on the self-consistent mean-field level and collective methods that extend the approach beyond the mean-field approximation differ in the functional dependence on the nucleonic densities and currents and contain model parameters. The most efficient functional density dependence and the values of most parameters, even though constrained to a certain extent by the microscopic dynamics, ultimately have to be determined by low-energy data.

In the first part of this study [1], we have used concepts from information geometry to analyze a representative semiempirical functional and show that, in general, nuclear EDFs are "sloppy" [2–6]. This means that even when their parameters are adjusted to data, the predictions of nuclear EDFs and related models are sensitive to only a few combinations of parameters (*stiff* parameter combinations) and exhibit an exponential decrease of sensitivity to variations of the remaining *soft* parameters that are only approximately constrained by data. By considering the space of model predictions as a manifold embedded in the data space, we have shown that the exponential distribution of model manifold widths corresponds to the range of parameter sensitivity. These results indicate that most nuclear EDFs, if not all, in fact contain models of lower effective dimension associated with the stiff combinations of model parameters.

A systematic simplification of the complex dependence on nucleonic densities and currents of a sloppy EDF, and the reduction of the model to a lower dimension in parameter space, crucially depends on the selection of data that constrain the functional form and determine parameter values. In Ref. [1], we have employed the manifold boundary approximation method (MBAM) [3] to deduce the most effective functional form of the density-dependent coupling parameters of a representative model EDF. However, since the application of MBAM necessitates the computation of both first and second derivatives of observables with respect to model parameters along geodesic paths on the model manifold, the data used in Ref. [1] included only a set of points on a microscopic equation of state (EoS) of symmetric nuclear matter and neutron matter. In that case, derivatives of pseudo-observables with respect to model parameters can be evaluated analytically, and the computational task of applying the MBAM to the nuclear system is not particularly difficult. On the downside, such a study is not very realistic because it does not include data on finite nuclei that are almost always used to determine or fine-tune the parameters of an EDF.

In this work, we extend the study of Ref. [1] and use a simple numerical approximation that enables the application of the MBAM to realistic nuclear energy density functionals, constrained not only by the nuclear matter EoS but also by observables that can be measured in nuclei all over the mass table. We will start from the same model EDF and microscopic EoS as in Ref. [1] and include additional ground-state properties of spherical nuclei in the set of data used to determine the functional form and model parameters. The aim is to show how methods of information geometry, and the MBAM in particular, can be employed to construct and optimize nuclear energy density functionals. Section II defines the model functional and describes the data set used in the analysis of parameter sensitivity. In Sec. III we apply the MBAM in a reduction of the parameter space dimension and the corresponding transformation of the functional density dependence. Section IV contains a summary and conclusions.

II. THE FUNCTIONAL DD-PC1 AND THE DATA SET

As representative of a class of semiempirical energy density functional that are currently used in numerous studies of nuclear structure phenomena, also in this work we consider

the relativistic functional DD-PC1 [7]. It explicitly includes nucleon degrees of freedom only and is constructed with second-order interaction terms; that is, the functional contains interaction terms bilinear in the densities and currents in the isoscalar-scalar, isoscalar-vector, and isovector-vector isospace-space channels. Many-body correlations are encoded in the density-dependent coupling functions:

$$\alpha_s(\rho) = a_s + (b_s + c_s x)e^{-d_s x},$$
$$\alpha_v(\rho) = a_v + b_v e^{-d_v x}, \qquad (1)$$
$$\alpha_{tv}(\rho) = b_{tv} e^{-d_{tv} x},$$

where the indices s, v, and tv denote the isoscalar-scalar, isoscalar-vector, and isovector-vector channels, respectively. $x = \rho/\rho_{\text{sat}}$, where ρ_{sat} indicates the nucleon density at saturation in symmetric nuclear matter. The corresponding Lagrangian contains an additional derivative term with a single constant parameter [7] that accounts for leading effects of finite-range interactions and is essential for a quantitative description of nuclear density distributions. From a Lagrangian with bilinear interaction terms, one derives the linear single-nucleon Dirac (Kohn-Sham) equation which, because of the density dependence of the couplings, contains also rearrangement terms. Like for other similar nuclear energy density functionals, both relativistic and nonrelativistic, the explicit medium dependence of the couplings can be derived, at least in principle, from the underlying microscopic internucleon interactions. However, the strength parameters of the functional, and in the present case there are ten parameters, are adjusted directly to nuclear data. In recent studies of global performance of relativistic EDFs in modeling ground-state properties of even-even nuclei over the entire mass table [8,9], it has been shown that DD-PC1 is currently one of the most accurate functionals, comparable in predictions to the latest Skyrme and Gogny nonrelativistic functionals.

In this study, we also consider properties of open-shell nuclei and, therefore, in addition to the effective interaction in the particle-hole channel, pairing correlations must be taken into account. The relativistic Hartree-Bogoliubov (RHB) model [10] will be used in self-consistent mean-field calculations of ground-state properties. As in many recent nuclear structure applications of the RHB framework based on the functional DD-PC1 [11], for the pairing interaction we employ a finite-range force that is separable in momentum space and is completely determined by two parameters adjusted to reproduce the result of the D1S Gogny interaction for the density dependence of the bell-shaped pairing gap in nuclear matter [12]. The present analysis of parameter sensitivity of the functional DD-PC1 does not include the pairing interaction; that is, the parameters of the pairing force are kept constant while the functional form of the density dependence and strength parameters of the EDF are modified and adjusted to reproduce the data.

Extending the analysis of Ref. [1] to include data on finite nuclei, the (pseudo-) observables that determine the parameters of the functional consist of two sets of data. The first contains seven points of the microscopic equation of state of symmetric nuclear matter and six points of the neutron matter equation of state of Ref. [13], based on the

TABLE I. Pseudodata for infinite symmetric nuclear matter used to compute the penalty function χ^2 for the energy density functional defined by Eq. (1). The seven points of energy as function of the nuclear matter density correspond to the microscopic EoS of Ref. [13]. In the least-squares fit the adopted error for the EoS points is 10%.

Pseudo-observable	
$\epsilon(0.04 \text{ fm}^{-3})$	-6.48 MeV
$\epsilon(0.08 \text{ fm}^{-3})$	-12.43 MeV
$\epsilon(0.12 \text{ fm}^{-3})$	-15.43 MeV
$\epsilon(0.16 \text{ fm}^{-3})$	-16.03 MeV
$\epsilon(0.20 \text{ fm}^{-3})$	-14.99 MeV
$\epsilon(0.24 \text{ fm}^{-3})$	-12.88 MeV
$\epsilon(0.32 \text{ fm}^{-3})$	-6.49 MeV

Argonne $V_{18} NN$ potential and the Urbana model IX (UIX) three-nucleon interaction. One could, of course, use any other microscopic EoS of nuclear and neutron matter. As this study aims to demonstrate the applicability of the MBAM to nuclear density functionals rather than to uniquely determine the parameters of a functional, the choice of the microscopic EoS is not essential for the present discussion. In addition to the pseudo-observables of the infinite homogeneous nuclear medium, the second set of data contains ground-state properties of eight spherical nuclei: binding energies, charge radii, and available data on the difference between radii of neutron and proton distributions. Additional nuclei and data points could be included in a more quantitative analysis. Here, we are interested not so much in an accurate determination of model parameters but rather in qualitative constraints on the functional form of the density dependence. The relatively small set selected for the present analysis extends, nevertheless, from ^{16}O to ^{214}Pb and includes both closed-shell and single open-shell nuclei. The data that will be used to analyze the functional form of DD-PC1 are listed in Tables I–III.

The set of all possible values of model parameters defines the 10-dimensional manifold embedded in the N-dimensional data space ($N = 29$ in the present case). For a given point in the data space, that is, for the set of data listed in Tables I–III,

TABLE II. Pseudo-data for neutron matter used to compute the penalty function χ^2 for the energy density functional defined by Eq. (1). The six points correspond to the microscopic neutron matter EoS of Ref. [13]. In the least-squares fit, the adopted error for the energy of pure neutron matter as a function of density is 10%.

Pseudo-observable	
$\epsilon(0.04 \text{ fm}^{-3})$	6.45 MeV
$\epsilon(0.08 \text{ fm}^{-3})$	9.65 MeV
$\epsilon(0.12 \text{ fm}^{-3})$	13.29 MeV
$\epsilon(0.16 \text{ fm}^{-3})$	17.94 MeV
$\epsilon(0.20 \text{ fm}^{-3})$	22.92 MeV
$\epsilon(0.24 \text{ fm}^{-3})$	27.49 MeV

TABLE III. The total binding energies BE, charge radii r_{ch}, and the differences between the radii of neutron and proton density distributions $r_{np} = r_n - r_p$ used to compute the penalty function χ^2 for the energy density functional defined by Eq. (1). The adopted errors for the binding energies and charge radii are 0.1% and 0.2%, respectively, while 5% is assumed for the accuracy of the neutron skin values.

Nucleus	BE (MeV)	r_{ch} (fm)	$r_n - r_p$ (fm)
^{16}O	−127.619 MeV	2.73	
^{48}Ca	−415.991 MeV	3.484	
^{72}Ni	−613.173 MeV		
^{90}Zr	−783.893 MeV	4.272	
^{116}Sn	−988.681 MeV	4.626	0.12
^{132}Sn	−1102.860 MeV		
^{208}Pb	−1636.446 MeV	5.505	0.20
^{214}Pb	−1663.298 MeV	5.562	

the nine parameters that determine the density dependence of the coupling functions Eq. (1), plus the strength parameter of the derivative term $\delta_s(\partial_\nu \bar{\psi}\psi)(\partial^\nu \bar{\psi}\psi)$ of the functional DD-PC1, are optimized by minimizing the penalty function $\chi^2(\mathbf{p})$ on the manifold of model predictions embedded in the data space:

$$\chi^2(\mathbf{p}) = \sum_{n=1}^{N} r_n^2(\mathbf{p}), \qquad (2)$$

where $r_n(\mathbf{p})$ denotes the residual

$$r_n(\mathbf{p}) = \frac{\mathcal{O}_n^{(\mathrm{mod})}(\mathbf{p}) - \mathcal{O}_n}{\Delta\mathcal{O}_n}, \qquad (3)$$

and $\mathcal{O}_n^{(\mathrm{mod})}$ are model predictions that depend on the set of parameters $\mathbf{p} = \{p_1, \ldots, p_F\}$. Every observable is weighted by the inverse of $\Delta\mathcal{O}_n$, and the adopted errors are given in the captions to Tables I–III. The behavior of the model around the best-fit point $\mathbf{p}_0$ can be analyzed in the quadratic approximation to the penalty function:

$$\Delta\chi^2(\mathbf{p}) = \chi^2(\mathbf{p}) - \chi^2(\mathbf{p}_0) = \frac{1}{2}\Delta\mathbf{p}^T \hat{\mathcal{M}} \Delta\mathbf{p}, \qquad (4)$$

where $\Delta\mathbf{p} = \mathbf{p} - \mathbf{p}_0$. The curvature matrix

$$\mathcal{M}_{\mu\nu} = \left.\frac{\partial^2 \chi^2}{\partial p_\mu \partial p_\nu}\right|_{\mathbf{p}=\mathbf{p}_0} \qquad (5)$$

is symmetric and can be diagonalized by an orthogonal transformation: $\hat{\mathcal{M}} = \hat{\mathcal{A}}\hat{\mathcal{D}}\hat{\mathcal{A}}^T$, where $\hat{\mathcal{A}}$ denotes the orthogonal matrix with columns corresponding to normalized eigenvectors of $\hat{\mathcal{M}}$, and the diagonal matrix $\hat{\mathcal{D}}$ contains the eigenvalues of $\hat{\mathcal{M}}$. The deviation of χ^2 from its minimum value can be expressed as

$$\Delta\chi^2(\mathbf{p}) = \frac{1}{2}\Delta\mathbf{p}^T(\mathcal{A}\mathcal{D}\mathcal{A}^T)\Delta\mathbf{p} = \frac{1}{2}\xi^T\mathcal{D}\xi = \frac{1}{2}\sum_{\alpha=1}^{F}\lambda_\alpha\xi_\alpha^2. \qquad (6)$$

The transformed vectors $\xi = \hat{\mathcal{A}}^T\mathbf{p}$ define the principal axes on the F-dimensional model manifold. Figure 1 displays the eigenvectors and eigenvalues of the 10×10 Hessian matrix

of second derivatives $\mathcal{M}$ of $\chi^2(\mathbf{p})$ at the best-fit point for the functional defined by the couplings of Eq. (1), plus the strength parameter of the derivative term δ_s. We will refer to this set of parameters as set 1. The empty and filled bars indicate that the corresponding amplitudes contribute with opposite signs. The eigenvalues of the Hessian matrix, characterizing the sensitivity of model predictions to variations along orthogonal directions in parameter space, span ten orders of magnitude, and this is typical of sloppy models that exhibit an exponentially large range of sensitivities to changes in parameter values [2,4,5,14–16]. Such a model is essentially determined by only a few *stiff* directions in parameter space characterized by large eigenvalues λ_α, while the remaining *soft* directions that correspond to small eigenvalues λ_α are not constrained by the data used in the least-squares fit.

III. MODEL REDUCTION BY THE MANIFOLD BOUNDARY APPROXIMATION METHOD

In Ref. [1] we have also shown that the functional DD-PC1 exhibits another unique characteristic of sloppy models [2,3,5,6], namely that the widths of the model manifold in the directions of the eigenvectors of the Hessian follow closely the distribution of sensitivity (square root of the eigenvalue of the Hessian) of the functional to changes in the values of the corresponding parameter combinations. By interpreting the space of model predictions as a manifold embedded in the Euclidean data space, with parameters of the functional as coordinates on the manifold, one can explore the boundaries of the manifold using geodesic paths. Boundaries correspond to points on the manifold where the metric becomes singular, and the arc length of geodesics, along directions specified by the eigenvectors of the Hessian matrix at the minimum of χ^2, provide a measure of the manifold width in each of these directions [5]. The parameters corresponding to a geodesic path can be found as the solution of the second-order differential equation

$$\ddot{p}_\mu + \sum_{\alpha\beta} \Gamma_{\alpha\beta}^\mu \dot{p}_\alpha \dot{p}_\beta = 0, \qquad (7)$$

where $\Gamma_{\alpha\beta}^\mu$ are the connection coefficients:

$$\Gamma_{\mu\nu}^\alpha = \sum_\beta (g^{-1})_{\alpha\beta} \sum_m \frac{\partial r_m}{\partial p_\beta} \frac{\partial^2 r_m}{\partial p_\mu \partial p_\nu}, \qquad (8)$$

the metric on the model manifold is defined by the Fisher information matrix (FIM):

$$g_{\mu\nu} = \sum_m \frac{\partial r_m}{\partial p_\mu} \frac{\partial r_m}{\partial p_\nu}, \qquad (9)$$

and the dot denotes differentiation with respect to the affine parametrization of the geodesic. Note that at the best-fit point (minimum of χ^2), the metric $g_{\mu\nu}$ of the model manifold approximately equals the Hessian matrix of second derivatives $\mathcal{M}$ of $\chi^2(\mathbf{p})$. The geodesic equation presents an initial value problem in the parameter space. Starting from any point on the model manifold, one follows the geodesic path in a
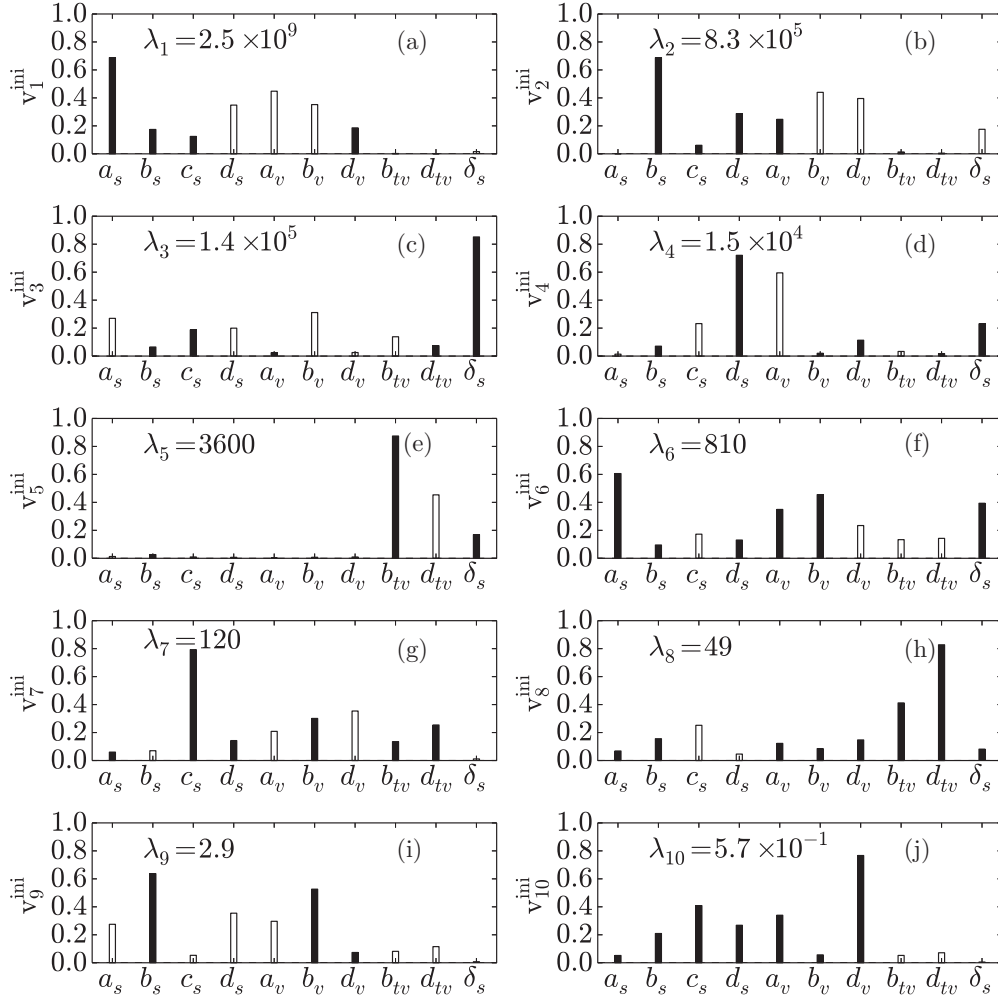
FIG. 1. Eigenvectors and eigenvalues of the 10×10 Hessian matrix of second derivatives $\mathcal{M}$ of $\chi^2(\mathbf{p})$ at the best-fit point for the functional defined by the couplings of Eq. (1), plus the strength parameter of the derivative term δ_s. The empty and filled bars indicate that the corresponding amplitudes contribute with opposite signs.

given direction until the boundary is identified by the metric tensor becoming singular. In particular, if one considers the best-fit point $\chi^2(\mathbf{p}_0)$, the geodesic equation can be integrated along the eigendirection of the Hessian matrix to determine the corresponding boundaries of the model manifold. The initial value $\mathbf{p}_{\text{ini}}$ corresponds to the best-fit parameters, and the initial velocities $\dot{\mathbf{p}}_{\text{ini}}$ are determined by the eigenvectors of the Hessian at the best-fit point. An eigenvector defines two possible directions for integration (positive and negative), and the sum of the two arc lengths equals the width of the manifold for that particular eigendirection [3].

In the analysis of the DD-PC1 model manifold of Ref. [1], we have only considered a set of pseudo-observables, energies as function of density, for infinite nuclear matter. In this case, the derivatives of residuals with respect to model parameters, contained in the expression for the connection coefficients (8), can be calculated analytically. Here. the data set is extended with ground-state properties of finite nuclei for which the connection coefficients have to be calculated numerically. The computational task can be considerably reduced by interchanging the order of summations implicit in Eqs. (7)

and (8), that is, by calculating first the following quantity:

$$\sum_{\alpha\beta} \frac{\partial^2 r_m}{\partial p_\alpha \partial p_\beta} \dot{p}_\alpha \dot{p}_\beta = \|\dot{\mathbf{p}}\|^2 \sum_{\alpha\beta} \frac{\partial^2 r_m}{\partial p_\alpha \partial p_\beta} \frac{\dot{p}_\alpha}{\|\dot{\mathbf{p}}\|} \frac{\dot{p}_\beta}{\|\dot{\mathbf{p}}\|}$$

$$= \frac{\|\dot{\mathbf{p}}\|^2}{\epsilon^2} \sum_{\alpha\beta} \frac{\partial^2 r_m}{\partial p_\alpha \partial p_\beta} \delta p_\alpha \delta p_\beta, \quad (10)$$

where

$$\delta p_\mu \equiv \epsilon \frac{\dot{p}_\mu}{\|\dot{\mathbf{p}}\|}, \quad \mu \in \{\alpha, \beta\}, \quad (11)$$

and ϵ is a small constant. A Taylor expansion for the residual r_m leads to the following expression:

$$\sum_{\alpha\beta} \frac{\partial^2 r_m}{\partial p_\alpha \partial p_\beta} \delta p_\alpha \delta p_\beta \approx r_m(p_1 + \delta p_1, \ldots, p_n + \delta p_n)$$

$$+ r_m(p_1 - \delta p_1, \ldots, p_n - \delta p_n)$$

$$- 2 r_m(p_1, \ldots, p_n). \quad (12)$$

The calculation is simplified by numerically computing directional second-order derivatives instead of all second derivatives entering the definition of connection coefficient. The initial nine parameters defined in Eq. (1), plus the strength parameter of the derivative term δ_s, are transformed as follows:

$$a_s = a_{s,bf}\, p_{a_s}, \quad b_s = b_{s,bf}\, p_{b_s},$$
$$c_s = c_{s,bf}\, p_{c_s}, \quad d_s = d_{s,bf}\, p_{d_s}, \tag{13}$$

$$a_v = a_{v,bf}\, p_{a_v}, \quad b_v = b_{v,bf}\, p_{b_v}, \quad d_v = d_{v,bf}\, p_{d_v}, \tag{14}$$

$$b_{tv} = b_{tv,bf}\, p_{b_{tv}}, \quad d_{tv} = d_{tv,bf}\, p_{d_{tv}}, \tag{15}$$

$$\delta_s = \delta_{s,bf}\, p_{\delta_s}. \tag{16}$$

where the subscript bf denotes the best-fit values obtained by minimizing the penalty function $\chi^2(\mathbf{p})$ (set 1). In this way, all the parameters in the geodesic equation (7) become dimensionless, and their values at the initial point:

$$p_\mu(0) = 1, \quad \mu \in \{a_s, b_s, c_s, d_s, a_v, b_v, d_v, b_{tv}, d_{tv}, \delta_s\}. \tag{17}$$

Compared to the transformation we used in the previous study (see Appendix B of Ref. [1]), here the parameters are not constrained to have the same sign along the geodesic path. This allows us to explore the entire parameter space and, by including data on finite nuclei, the data space contains enough points to avoid possible unphysical regions of parameters. The initial velocities are determined by the corresponding amplitudes of eigenvectors of the Hessian matrix ($\mathcal{M} = \mathcal{A}\mathcal{D}\mathcal{A}^T$) of the penalty function (cf. Fig. 1):

$$\dot{p}_\mu(0) \sim \mathcal{A}_\mu. \tag{18}$$

The overall normalization factor is chosen so that the data space norm of the velocity vector equals one,

$$\sum_{\mu,\nu} g_{\mu\nu} \dot{p}_\mu(0) \dot{p}_\nu(0) = 1, \tag{19}$$

and $g_{\mu\nu}$ denotes the metric tensor (FIM). Because an eigenvector is defined up to an overall phase, Eqs. (18) and (19) determine two opposite directions for the initial velocity. For each direction, the geodesic equation is integrated up to the manifold boundary and, since the data space norm of the velocity remains constant, the length of the traversed path in the data space equals the maximal value of the affine parameter. The sum of the two arcs equals the width of the model manifold for this particular combination of bare model parameters.

The resulting widths of the model manifold in the directions of eigenvectors of the Hessian matrix of the penalty function $\chi^2(\mathbf{p}_0)$ exhibit an exponential distribution of values (cf. Fig. 1 in Ref. [1]), and this points to the existence of an effective functional of lower dimension associated with stiff parameter combinations. The reduction of a general sloppy model to lower dimension in parameter space is essentially determined by the choice of data to which the parameters are adjusted. Following our study of DD-PC1 in nuclear matter in Ref. [1], we employ the manifold boundary approximation method (MBAM) [3] to construct a simpler EDF of lower parameter space dimension, constrained by the data set listed in Tables I–III, and which also includes ground-state data of finite nuclei.
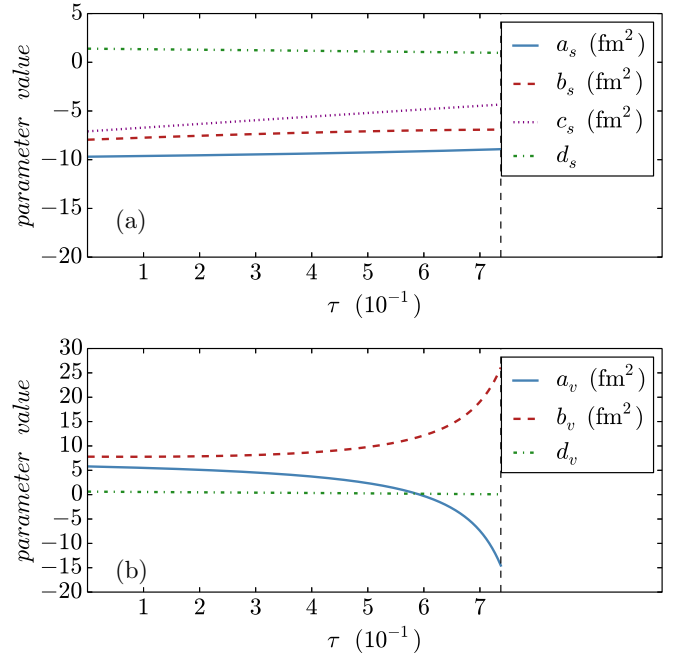

FIG. 2. The parameters of the isoscalar part of the ten-parameter functional set 1, as functions of the affine parametrization, along the geodesic path determined by the eigenvector of the Hessian matrix that corresponds to the smallest eigenvalue (cf. Fig. 1). Panel (a) displays the four parameters of the scalar channel, while the evolution of the three parameters that determine the vector channel is shown in panel (b).

Starting from the best-fit point $\mathbf{p}_0$ in parameter space, the geodesic equation is integrated in the eigendirection that corresponds to the smallest eigenvalue of the Hessian matrix, until the boundary of the model manifold is reached. Because the eigenvector is defined up to an overall phase, we choose the direction in which the parameter space norm of the velocity vector ($\sum_\mu \dot{p}_\mu^2$) increases [1,3]. The model limit associated with the manifold boundary is analyzed and a different model is constructed that contains one less parameter. This model is then optimized by a least-squares fit to the same set of data and used as a starting point for the next iteration of the MBAM. This method, therefore, reduces the sloppiness of a model by successively eliminating soft combinations of bare parameters. In the ideal case in which the data set contains all the information necessary to completely determine an *a priori* unknown physical model, the MBAM will produce a unique nonsloppy model with only stiff combinations of bare parameters.

The first iteration of the MBAM for the initial ten-parameter functional is illustrated in Figs. 2–4. The evolution of the parameters along the geodesic path determined by the eigenvector of the Hessian matrix that corresponds to the smallest eigenvalue, as functions of the affine parametrization of the geodesic, is shown in Figs. 2 and 3. The geodesic equation is integrated with the initial conditions described above until the corresponding boundary of the model manifold is identified. While there are no significant changes of the parameters in the isoscalar-scalar and isovector-vector channels, as well as the
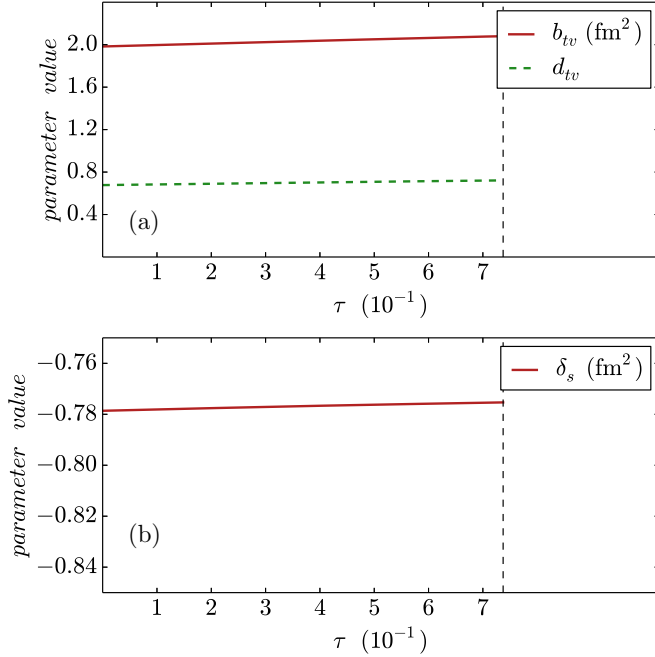
FIG. 3. Same as in the caption to Fig. 2 but for the two parameters of the isovector part of the functional defined in Eq. (1) (a) and the strength parameter of the derivative term (b).
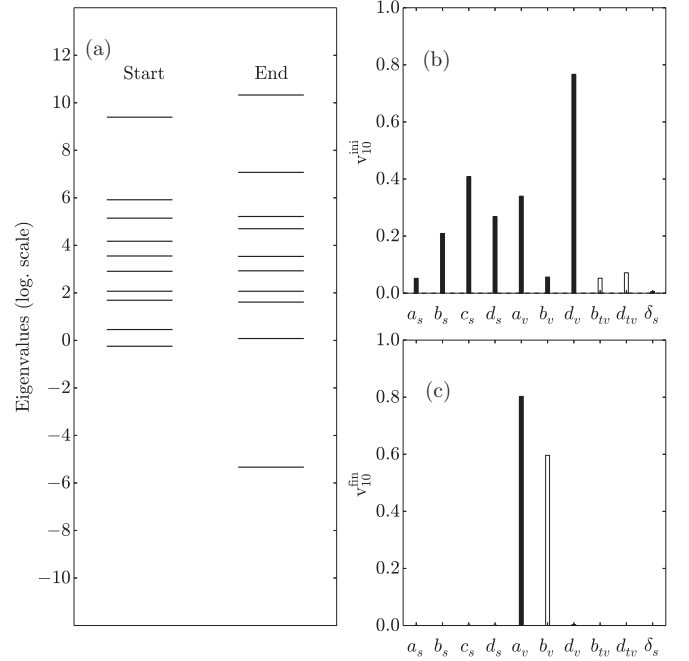

FIG. 4. The initial (best-fit point) and final (at the boundary of the model manifold) eigenspectrum of the FIM for the ten-parameter functional SET 1 (a). The eigenvectors that correspond to the initial and final smallest eigenvalues are shown in panels (b) and (c).

strength of the derivative term, in the isoscalar-vector channel one notes that the parameters a_v and b_v start to diverge as the geodesic path approaches the boundary of the manifold, and d_v tends to a small value close to zero. This can be understood from the form of the vector coupling:

$$\alpha_v(\rho) = a_v + b_v e^{-d_v x}, \quad x = \rho/\rho_{\text{sat}}. \tag{20}$$

When d_v approaches zero, the derivatives $\partial \alpha_v/\partial a_v$ and $\partial \alpha_v/\partial b_v$ are virtually identical, the corresponding rows and columns of the FIM are almost equal, and the matrix becomes singular. In Fig. 4(a) we plot the initial and final (at the boundary) eigenspectrum of the FIM, and the initial and final eigenvectors that correspond to the smallest eigenvalues in Figs. 4(b) and 4(c). At the boundary, the smallest eigenvalue separates from the rest of the spectrum and tends to zero. While all bare parameters, with the exception of δ_s, contribute to the amplitudes of the initial softest eigenvector, at the boundary only the components a_v and b_v (with opposite phases) determine the eigenvector of the FIM with the eigenvalue approaching zero. The limiting behavior of a_v, b_v, and d_v suggests the following Taylor expansion for the vector coupling function at the boundary:

$$\alpha_v(\rho) \approx a_v + b_v(1 - d_v x) = a_v + b_v - b_v d_v x = \tilde{a}_v + \tilde{b}_v x. \tag{21}$$

In first order, this reduces the functional form of the coupling function in the isoscalar-vector channel to a linear density dependence, and the corresponding number of bare parameters from three to two. In the final step, the nine parameters of the resulting model are again determined in a least-squares fit to

the data listed Tables I–III (set 2) and used as a starting point for the next iteration of the MBAM.

The second iteration thus starts with a model functional determined by the nine parameters: $a_s, b_s, c_s, d_s, \tilde{a}_v, \tilde{b}_v, b_{tv}, d_{tv},$ and δ_s (set 2). The eigenvectors and eigenvalues of the FIM calculated at the best-fit point (Hessian matrix) are shown in Fig. 5. In this case, the eigenvalues span nine orders of magnitude. Starting from the best-fit point, the geodesic equation is integrated following the direction determined by the softest eigenvector, and in Figs. 6 and 7 we display the evolution of the model parameters, as functions of the affine parametrization of the geodesic. A scenario similar to the first iteration unfolds, only this time in the isoscalar-scalar channel. As the parameter of the exponential function d_s approaches zero, and the two parameters a_s and b_s start to diverge, the FIM becomes singular at the manifold boundary. The eigenvector with the smallest eigenvalue decouples from the rest, as shown in Fig. 8. The eigenvalue tends to zero, while the amplitudes of the corresponding eigenvector exhibit dominant out-of-phase components a_s and b_s. The initial and final eigenvalues of the FIM are displayed in Fig. 8(a).

The divergent behavior of the parameters a_s and b_s, and the Taylor expansion of the exponential coupling function to first order in the small parameter d_s at the boundary, lead to the following reduction of the isoscalar-scalar coupling function:

$$\begin{aligned}
\alpha_s(\rho) &\approx a_s + (b_s + c_s x)(1 - d_s x) \\
&= a_s + b_s + (c_s - b_s d_s)x - c_s d_s x^2 \\
&= \tilde{a}_s + \tilde{b}_s x + \tilde{c}_s x^2. \tag{22}
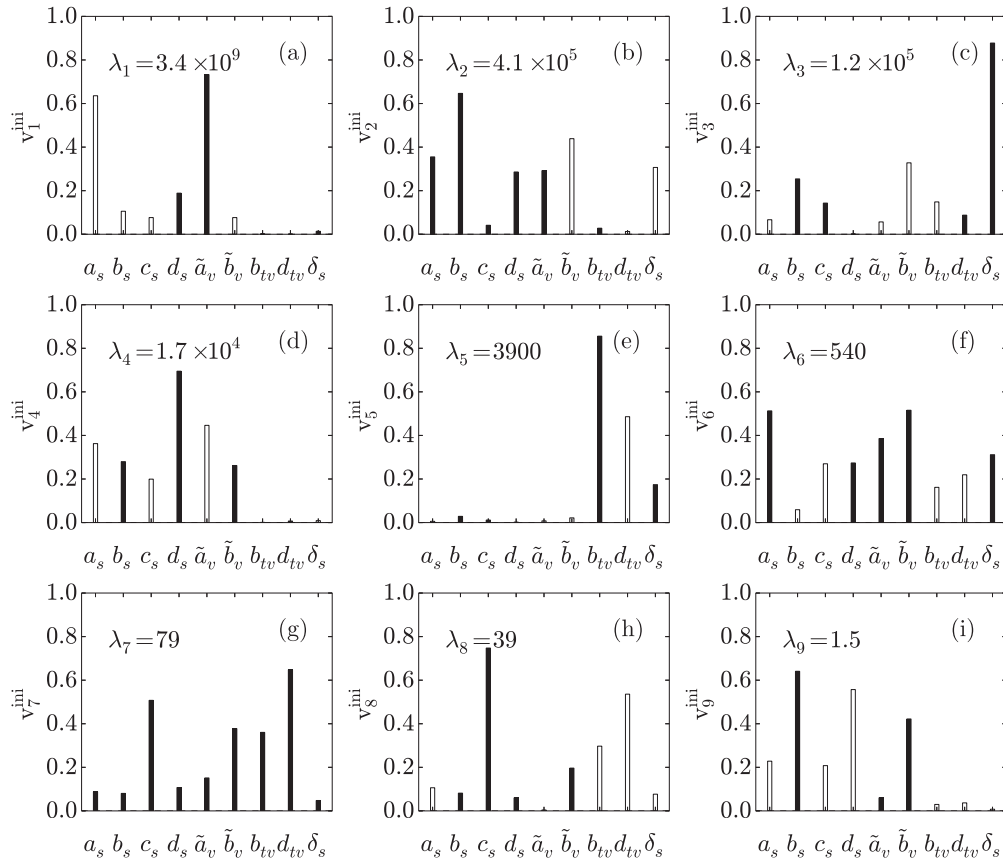\end{aligned}$$

FIG. 5. Same as in the caption to Fig. 1 but for the functional with nine parameters (set 2) obtained by applying the MBAM to the ten-parameter functional set 1.
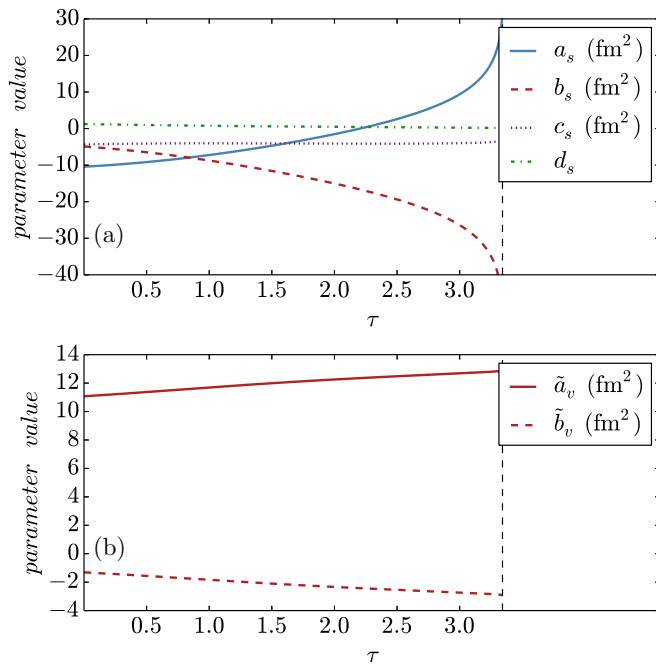

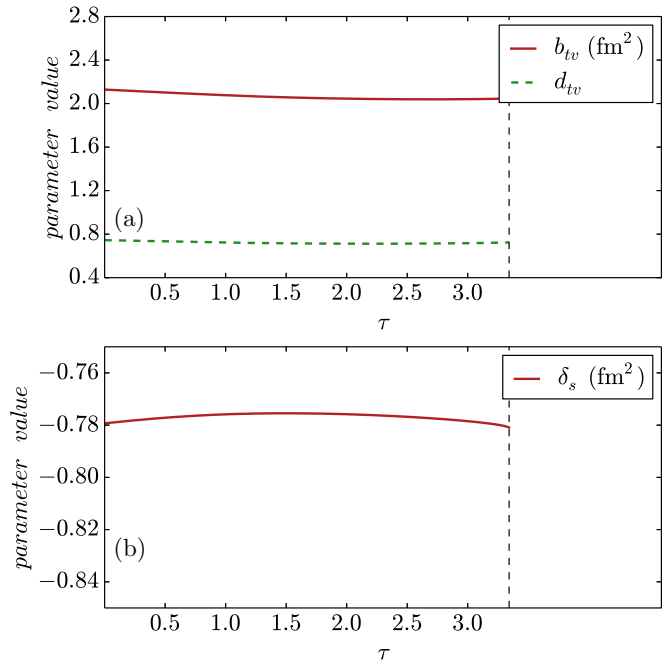FIG. 6. Same as in the caption to Fig. 2 but for the nine-parameter functional (set 2).

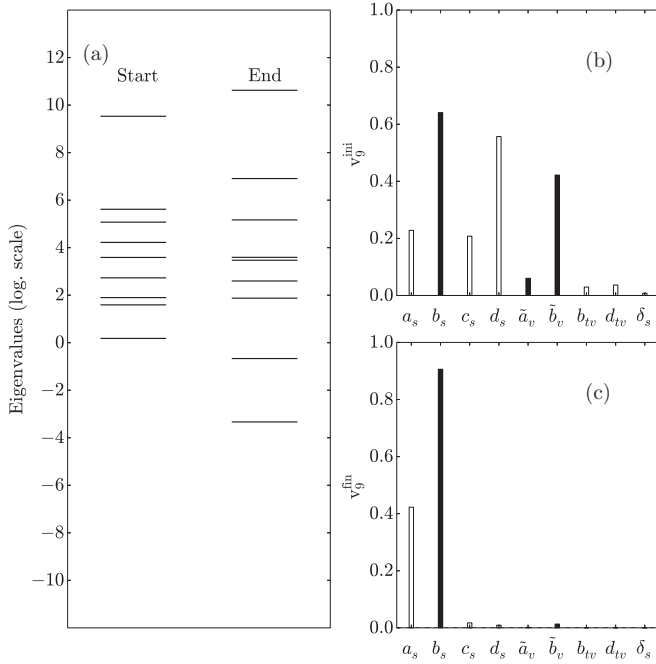FIG. 7. Same as in the caption to Fig. 3 but for the nine-parameter functional (set 2).

FIG. 8. Same as in the caption to Fig. 4 but for the nine-parameter functional (set 2).
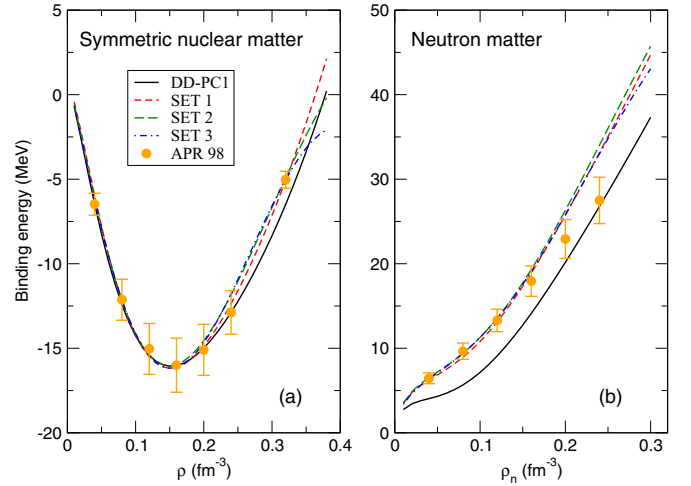

FIG. 9. Equation of state of symmetric nuclear matter (a) and neutron matter (b). Energy as a function of nuclear (neutron) matter calculated with the functional DD-PC1, and the three functionals adjusted in this study, sets 1, 2, and 3, are shown in comparison to the microscopic equations of state [13]. The points to which the parameters of the functionals have been fitted are shown with the adopted uncertainty 10%.

The second iteration, therefore, transforms the coupling in the isoscalar-scalar channel to a polynomial of second degree in the nucleonic density, and the number of parameters is reduced by one. As a final step of this MBAM iteration, the new model determined by the eight parameters $\tilde{a}_s$, $\tilde{b}_s$, $\tilde{c}_s$, $\tilde{a}_v$, $\tilde{b}_v$, b_{tv}, d_{tv}, and δ_s is again fitted to the observables listed in Tables I–III. The resulting parameters are denoted set 3.

Note that in both MBAM iterations the parameters of the isovector-vector channel b_{tv} and d_{tv}, as well as the strength parameter of the derivative term δ_s, do not display significant variations along the softest eigendirections (Figs. 3 and 7) or in the two successive least-squares adjustments to data. This means that the parameters of the isovector channel and the derivative term are already constrained by the data used in the fit (in particular, the neutron matter EoS and difference of the radii of neutron and proton distributions for the isovector channel, and charge radii for the derivative term). The dominant component of the third eigenvector of the Hessian matrix for both best-fit points (Figs. 1 and 5) corresponds to the bare parameter δ_s, while the fifth eigenvector is characterized by large out-of-phase amplitudes that correspond to b_{tv} and d_{tv}. To constrain the in-phase combination of the isovector parameters, additional data are required such as, for instance, information on the isovector effective mass in nuclear matter.

The functional determined by the eight parameters (five in the isoscalar channel):

$$\alpha_s(\rho) = \tilde{a}_s + \tilde{b}_s x + \tilde{c}_s x^2 \quad \text{and} \quad \alpha_v(\rho) = \tilde{a}_v + \tilde{b}_v x, \quad (23)$$

where $x = \rho/\rho_{\text{sat}}$, two in the isovector-vector channel b_{tv} and d_{tv}, and the parameter of the derivative term δ_s (set 3), could, in principle, be further reduced. However, for the data set of

Tables I–III, in the next, third iteration, the integration of the geodesic equation does not lead to the decoupling of the softest eigenvector. Even considering both directions determined by the softest eigenvector of the Hessian matrix, we have not been able to reach the corresponding boundary of the model manifold and, therefore, the number of parameters could not be reduced. Note that in our previous study [1], in which only nuclear matter pseudo-data were used to determine the parameters of the functional, it was possible to reduce both isoscalar coupling functions to a linear dependence of the nucleonic density; that is, a third iteration reduced the number of isoscalar parameters to four. Here, this is no longer possible because ground-state properties of finite nuclei are included in the data set and, with only a simple linear density dependence of the scalar and vector coupling functions, a self-consistent mean-field calculation based on such a functional could not reproduce the data.

This effect is illustrated in Figs. 9 and 10, in which we display the results for nuclear matter and finite nuclei obtained with the functionals determined by the parameters set 1 (ten parameters), set 2 (nine parameters), and set 3 (eight parameters), in comparison to the original functional DD-PC1 (ten parameters). Note that DD-PC1 was actually not adjusted to the nuclear matter EoS and/or spherical nuclei, but rather to the binding energies of 64 axially deformed nuclei in the mass regions $A \approx 150$–180 and $A \approx 230$–250 [7].

In Fig. 9, we plot the equation of state for symmetric nuclear matter [Fig. 9(a)] and neutron matter [Fig. 9(b)]. The curves calculated with DD-PC1 and the three functionals adjusted in this study (sets 1, 2, and 3), are compared to the microscopic equations of state [13]. All three functionals, adjusted to the points shown in the figure (with the adopted uncertainty of 10%), reproduce the equations of state with
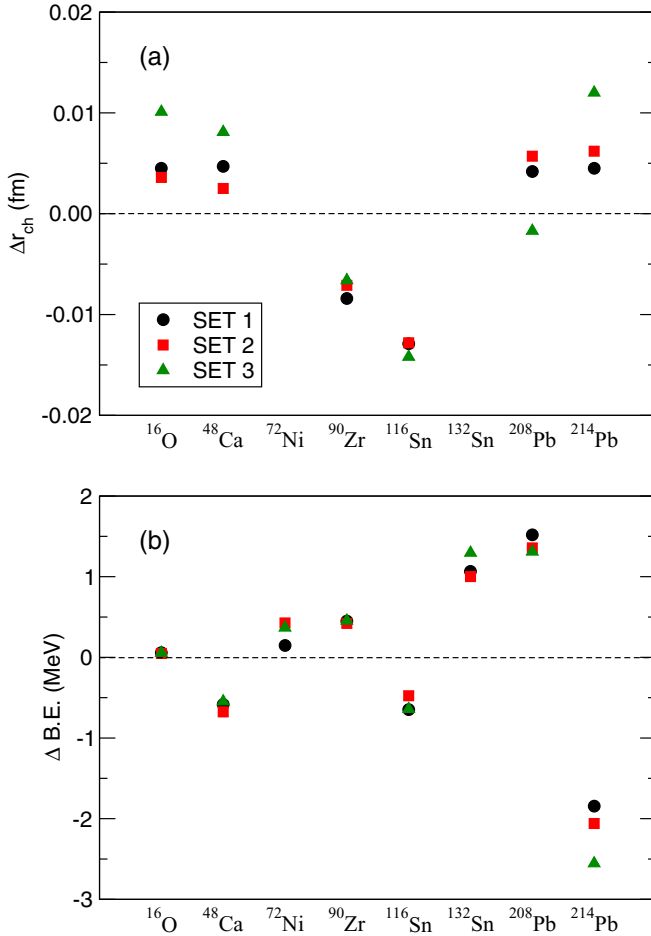
FIG. 10. Differences between the theoretical and experimental values for the charge radii (a) and binding energies (b) of the eight nuclei used to adjust the parameters of the functionals sets 1, 2, and 3.

comparable accuracy. It is only in the region of extrapolation at higher densities, where no fit points have been specified, that their predictions start to diverge. This is similar to the results obtained in Ref. [1]. DD-PC1 was not adjusted to these equations of state and, of course, does not reproduce the microscopic EoS particularly well, especially the EoS of neutron matter. Empirical properties of symmetric nuclear matter at saturation (binding energy, density, incompressibility), as well as two points at low and high density, are built into the parameters of DD-PC1 and, thus, this functional reproduces the microscopic EoS up to and slightly above saturation density. Figure 10 displays the absolute differences between the theoretical values and data for the charge radii and binding energies of the eight nuclei used in the least-squares fits of the parameter sets 1, 2, and 3. The binding energies are reproduced by all three functionals with similar accuracy, whereas several charge radii (^{16}O, ^{48}Ca, ^{208}Pb, and ^{214}Pb) calculated with the functional SET3 are markedly different from those predicted by sets 1 and 2. This already indicates that with a further reduction of the number of parameters it would not be possible to accurately reproduce the data set.

IV. SUMMARY AND OUTLOOK

One of the most important current research topics in low-energy nuclear physics is the development of a universal energy density functional framework that can be used in global studies of structure phenomena in different regions of the nuclear mass table. Even though structure models based on EDFs can accurately reproduce a variety of measured nuclear properties and in many cases provide useful predictions for regions far from stability where few data are available, empirically it has been known for a long time that nuclear EDFs exhibit an exponential range of sensitivity to parameter variations, crucially depend on just a few parameter combinations, while the remaining combinations of bare model parameters can only approximately be constrained by available data. Various approaches to the construction of EDFs lead to different, and sometimes very complex, functional dependence on nucleonic densities and currents, characterized by a relatively large number of parameters whose values are difficult to accurately determine either microscopically or from experiment. Parameter uncertainties and propagation of errors, as well as correlations between parameters, have been the subject of numerous recent studies in the framework of nuclear density functional theory (see, for instance, Ref. [17] and references cited therein).

In Ref. [1] and in this work, we have analyzed a representative semi-empirical relativistic EDF, with a microscopically motivated ansatz for the functional density dependence, and parameters determined by empirical properties of homogeneous nuclear matter and data on ground-state nuclear properties. If the space of model predictions is considered as a manifold embedded in the data space, with model parameters as coordinates of the manifold, geodesic paths can be used to explore the boundaries of the model manifold. These are defined by points on the manifold where the metric (Fisher information matrix) becomes singular. Starting from a best-fit point for a given model functional, obtained by minimizing the penalty function χ^2 that provides a measure of the distance in the data space between model predictions and the data point to which the model is fitted, one can explore the boundaries of the model manifold in the directions of eigenvectors of the Hessian matrix of second derivatives of χ^2 at minimum. In Ref. [1] we have shown that the widths of the manifold of predictions for the model functional, that is, the arc lengths of geodesics along the eigendirections of the Hessian matrix, exhibit an exponential distribution nearly identical to the exponential range of sensitivity of the model to parameter variations. This is characteristic of sloppy models and indicates that our model functional could contain functionals of lower effective dimension in parameter space that can equally well reproduce data and with parameters more tightly constrained by the data.

The general problem of a reduction of a nonlinear sloppy model functional to lower dimensions in parameter space is difficult and depends on the data that are used to determine both the functional form of the density dependence as well as the values of the parameters. The solution cannot be found by simply eliminating bare model parameters but necessitates often nonlinear transformations in parameter space that also

modify the form of density dependence. We have shown that the recently introduced manifold boundary approximation method (MBAM) [3] can be used to systematically reduce the complexity and the sloppiness of a general nuclear EDF, with reduced sets of parameters constrained by the underlying microscopic dynamics and fine-tuned to nuclear data. While in Ref. [1] we only considered a set of pseudo-observables that characterize the microscopic EoS of nuclear matter, in the present study the data set has been extended with points on the microscopic EoS of neutron matter and ground-state properties (binding energies, charge radii, difference between radii of neutron and proton distributions) of eight spherical nuclei. Since first and second derivatives of observables with respect to parameters along geodesic paths on the model manifold have to be computed, the inclusion of data on finite nuclei makes the application of the MBAM computationally much more challenging. Nevertheless, it has been possible to reduce our original ten-parameter functional to an eight-parameter functional that reproduces the given data set with comparable accuracy. An important result is that the functional density dependence of the coupling functions (density-dependent parameters) has been simplified to a polynomial form in the isoscalar channel of the functional. After two MBAM iterations, in the third the algorithm could no longer identify the boundary of the model manifold in the direction of the softest eigenvector of the Hessian matrix and, therefore, the dimension of the parameter space could not be reduced further. This is one MBAM iteration less than in our previous study [1], in which only pseudodata on nuclear matter were used in the nonlinear least-squares fit. Obviously the additional data on finite nuclei place more stringent constraints on the functional form and parameter values, especially in the isoscalar channel, and thus prevent further parameter reduction.

Even though we have only analyzed a single representative example of semi-empirical functionals currently used in nuclear structure studies, the illustrative study has shown how the MBAM can be used in the development and optimization of nuclear EDFs. In particular, this method can be applied to fully microscopic functionals that encode the underlying many-body dynamics in a complex dependence on nucleonic densities and currents and include all terms allowed by symmetries. Generally such a functional will be characterized by a rather large number of parameters whose values have to be determined by low-energy data and, therefore, one expects that a microscopic derivation will produce a sloppy functional. When the complexity and parameter space of a general sloppy functional is systematically reduced by applying the MBAM as described in this work, it is the data that such a model is designed to reproduce that determine not only the values of model parameters but also the optimal functional form of the density dependence.

[1] T. Nikšić and D. Vretenar, Phys. Rev. C **94**, 024333 (2016).

[2] M. K. Transtrum, B. B. Machta, K. S. Brown, B. C. Daniels, C. R. Myers, and J. P. Sethna, J. Chem. Phys. **143**, 010901 (2015).

[3] M. K. Transtrum and P. Qiu, Phys. Rev. Lett. **113**, 098701 (2014).

[4] R. N. Gutenkunst, J. J. Waterfall, F. P. Casey, K. S. Brown, C. R. Myers, and J. P. Sethna, PLoS Comput. Bio. **3**, 1871 (2007).

[5] M. K. Transtrum, B. B. Machta, and J. P. Sethna, Phys. Rev. Lett. **104**, 060201 (2010).

[6] M. K. Transtrum, B. B. Machta, and J. P. Sethna, Phys. Rev. E **83**, 036701 (2011).

[7] T. Nikšić, D. Vretenar, and P. Ring, Phys. Rev. C **78**, 034318 (2008).

[8] S. E. Agbemava, A. V. Afanasjev, D. Ray, and P. Ring, Phys. Rev. C **89**, 054320 (2014).

[9] S. E. Agbemava, A. V. Afanasjev, T. Nakatsukasa, and P. Ring, Phys. Rev. C **92**, 054310 (2015).

[10] D. Vretenar, A. V. Afanasjev, G. A. Lalazissis, and P. Ring, Phys. Rep. **409**, 101 (2005).

[11] T. Nikšić, D. Vretenar, and P. Ring, Prog. Part. Nucl. Phys. **66**, 519 (2011).

[12] Y. Tian, Z. Y. Ma, and P. Ring, Phys. Lett. B **676**, 44 (2009).

[13] A. Akmal, V. R. Pandharipande, and D. G. Ravenhall, Phys. Rev. C **58**, 1804 (1998).

[14] B. B. Machta, R. Chachra, M. K. Transtrum, and J. P. Sethna, Science **342**, 604 (2013).

[15] K. S. Brown and J. P. Sethna, Phys. Rev. E **68**, 021904 (2003).

[16] J. J. Waterfall, F. P. Casey, R. N. Gutenkunst, K. S. Brown, C. R. Myers, P. W. Brouwer, V. Elser, and J. P. Sethna, Phys. Rev. Lett. **97**, 150601 (2006).

[17] D. G. Ireland and W. Nazarewicz, J. Phys. G: Nucl. Part. Phys. **42**, 030301 (2015).